AAE

AERONAUTICAL AND ASTRONAUTICAL

ENGINEERING DEPARTMENT

ENGINEERING EXPERIMENT STATION, COLLEGE OF ENGINEERING, UNIVERSITY OF ILLINOIS, URBANA

Aeronautical and Astronautical Engineering Department
University of Illinois Urbana, Illinois

Technical Report AAE 77-14

UILU-Eng 77-0514

NASA Grant NGR 14-005-194
Allen I. Ormsbee, Principal Investigator

PROPELLER STUDY PART III

EXPERIMENTAL DETERMINATION OF THRUST AND TORQUE ON THE YO-3A AIRCRAFT

by

S. A. Siddiqi, K. R. Sivier and A. I. Ormsbee

University of Illinois
Urbana, Illinois

September 1977

EXPERIMENTAL DETERMINATION OF PROPELLER THRUST AND TORQUE ON A YO-3A AIRCRAFT

This study was concerned with the development of a method of measuring the propeller thrust and torque on a Lockheed YO-3A aircraft (Fig. 1) in flight.

This aircraft is powered by a Continental IO-360A engine rated at 157 kW at 2800 rpm. The engine drives a three bladed, constant speed Hartzell propeller, through a pulley and belt system that provides a 3.33:1 speed reduction ratio. The blade pitch is controlled by a Woodward governor that supplies pressurized engine oil to the propeller through the hollow propeller shaft.

Based on the data given in Ref. 1, and assuming no losses in the drive system, an estimated maximum of 140 kW is delivered to the propeller. At a maximum propeller shaft speed of 840 rpm this yields 1600 m-N as the maximum-torque transmitted by the shaft.

Again based on data from Ref. 1, the thrust required for level flight at sea-level is in the range of 1100 to 2200 N. Reference 1 does not give performance data for the three-bladed propeller, but an assumption of a propeller efficiency of 50% and a sea-level stalling speed of 31 m/s yields an estimated maximum thrust available of 2200 N. The instrumentation for measuring thrust hence was designed on the basis of a maximum thrust of 2200 N (higher thrust loads of up to 4400 N can be measured without modification of the instrumentation).

Two basic approaches were considered for the in-flight measurements of thrust and torque.

1. Airflow Measurements

An airflow survey behind the propeller will in theory allow the determination of the thrust and torque acting on the propeller (Ref. 2). However, this method requires several corrections for the flow interference effects of the rest of the aircraft. These correction factors require a knowledge of several aircraft related factors, such as the aircraft geometry and flight conditions. Not only would these factors be difficult to analyze but they can also change significantly with flight and ambient conditions. In view of the difficulties inherent in determining these correction factors with sufficent accuracy, this approach was judged unsuitable for the purposes of this project.

2. Mechanical Measurements

The propeller shaft is driven through a reduction system employing pulleys and belts. This isolates the propeller shaft from the engine shaft. Hence load cell measurements on the engine mounts, a method frequently used for such applications, were considered unsuitable as they would not provide thrust information. The propeller shaft of the YO-3A aircraft is illustrated in Fig. 2. Approximately 23 cm. of the propeller shaft is forward of the bearing and is easily acessible for use. The strains induced in the propeller shaft are directly proportional to the loads transmitted to it by the propeller. Thus instrumentation of this shaft with strain gauges, could, in principle, determine the strain contributions of the propeller thrust and torque. Some of the difficulties inherent in this method are that the strain contributions of the loads acting on the propeller shaft must be separated and their contributing loads identified. Shaft heating, due to proximity with the engine compartment and due to engine oil flow inside the shaft, was another potential area for difficulty.

PROPELLER SHAFT LOADS

The propeller shaft is subjected to five different types of loads under running conditions. These loads are given below. Table I summarizes the strains and stresses in the propeller shaft due to thrust, torque and bending.

1. The thrust load delivered to the shaft by the propeller is estimated to have a maximum value of 2200 N, inducing a maximum axial strain of 9 micro-strains in the shaft. This corresponds to a maximum axial stess level of 1.83 MPa.

2. The torque delivered to the propeller by the shaft is estimated to have a maximum value of 1600 m-N. This induces shear strains in the shaft of 750 micro-strains, corresponding to a maximun shear stress of 55.3 MPa.

3. Bending of the propeller shaft is caused by the weight of the propeller as well as variations in the propeller blade aerodynamic loading. The weight of the propeller assembly is estimated at 450 N, and the support bearing of the shaft was located about 40 cm. away from the propeller. Thus the

bending moment produced at the bearing has a maximum value of about 180 m-N. This bending induces maximum axial strains of about 60 micro-strains in the shaft, corresponding to shaft axial stresses of about 1.25 MPa.

4. The shaft rotation also causes centrifugal loads. At a maximum shaft speed of 840 rpm the outer surface is under an acceleration of 24 g's. The resulting strains and stresses in the shaft are negligible compared to the strains and stresses caused by the other loads. Other possible sources of centrifugal loading are eccentricity in the shaft and dynamic mass unbalance in the propeller and shaft combination. These loads also produce negligible strains under normal operating conditions.

5. The internal oil pressure in the shaft directly induces both a circumferential loading of the shaft and an axial loading of the shaft. The circumferential loading produces a hoop stress (tension) in the shaft and through the Poisson effect induces an axial compressive stress. The effect of the oil pressure on the propeller hub produces an axial tension which opposes the above compressive stress. The net stress is about .21 MPa for an estimated maximum oil pressure of about .69 MPa. Hence this loading too may be ignored as compared to the thrust, torque

and bending loads.

Calibration tests performed on the aircraft confirmed that centrifugal loads and the internal oil pressure indeed induced negligible strains as compared to those caused by thrust, torque and bending.

From Table I it is observed that the ratios of the maximum strains due to thrust, bending, and torque are

$$\varepsilon_{T_{max}} : \varepsilon_{B_{max}} : \varepsilon_{Q_{max}} :: 1:6 : 42.4$$

These ratios illustrate the crux of the direct measurement problem; i.e., the presence of very low thrust strains in the presence of much larger bending and torque strains. The bending and torque transducers measure the bending and torque independent of the thrust and other loads. The thrust transducer, however, does not measure thrust independent of the other loads. Calibrations showed that there was a sizable torque interaction in the thrust signal, but the interaction of the bending and the other loads present in the thrust signal was found to be negligible. For a detailed discussion of the interactions of the other loads in the thrust signal see Ref.3, Sec. 3.2.5.

STRAIN GAUGE TRANSDUCER ARRANGEMENTS

The sensor arrangement to be used must be able to distinguish between the different loads present as well as to measure the load desired in a reliable, repeatable and accurate manner. The sensor must also be able to function over the range of environmental conditions met in flight.

In order to meet the above requirements strain gauges were chosen as the sensing elements for the transducer. Most strain gauge work is done in the 50 to 500 micro-strain range; within this range it is possible to measure changes of 2 to 5 micro-strains. The torque and bending strain levels are high enough to present no difficulties in their measurement. However, the thrust induced strain in the shaft has a maximum value of about 9 micro-strains (see Table I). This low level of strain poses problems for the thrust measurement.

The two approaches followed for the thrust measurement were (Fig. 3),

1) Mechanical intensification of the low level thrust strains. This approach was severely limited by the fact that operational reliability required that no modifications could be made to the shaft itself. Hence mechanical intensification was achieved by providing a weak link in parallel with the propeller shaft in the thrust load path. Fig. 4 gives a schematic diagram of such a system. The strain intensifier transducer is shown in Figs. 5 and 6. Foil strain gauges on the weak link were arranged in a full Wheatstone bridge, and they sensed the mechanically amplified strain. The intensifier was designed for an amplification of 40. However, in the labratory this system demonstrated a large torque strain interaction with the basic thrust strain (the torque strain was also amplified). This approach was hence dropped. For a more detailed description of the design and testing of this system see Ref. 3, Sec 3.2.4.

2) Direct shaft strain measurements were judged to be the most feasible method of measuring propeller thrust and torque. The most promising method was to use high-sensitivity semi-conducter strain gauges on the shaft to measure thrust. However these gauges have severe temperature characteristics. Foil gauges on the other hand are 50 to 80 times less sensitive but have no adverse temperature characteristics. Both of these methods were tested in the labratory. These tests showed that the semi-conductor strain gauges were preferable for reliable thrust measurements. The gauges used were matched sets of DGP-1000-500 gauges manufactured by Kulite Inc. (R=1000 ohms and Kg=155). For details of the comparision testing of the semi-conductor versus the foil strain gauges see Ref. 3, Sec 3.2.5.

Foil strain gauges can be used for the torque and bending transducers because of the relatively high strain levels involved. Each of these transducers consists of a Wheatstone bridge with an active strain gauge in each arm. Figure 7 illustrates the strains produced in the propeller shaft by thrust, torque and bending. Figure 8 shows the Wheatstone bridge arrangements for measuring each of these strains independently of the others. This independence is valid to the extent that the second order effects, non-linearities and cross-sensitivity of the gauges can be ignored. This also assumes that the gauges in each transducer are perfectly matched and that the strain field is uni-axial. For a more complete discussion of these bridge arrangements see Ref. 3,

Sec 3.2.3.

The transducer outputs are given by:

$$\text{THRUST } E_o = K_g[2(1 + \mu)\ \varepsilon_T]V$$

$$\text{TORQUE } E_o = K_g[2(1 + \mu)\ \varepsilon_Q]V$$

$$\text{BENDING } E_o = K_g\ [2(1 + \mu)\varepsilon_B]V$$

Table II gives the transducer sensitivities for each of these arrangements (for comparision the best results obtained with the weak link transducer are included).

The operating environment of these transducers is quite noisy in the electronic sense. Furthermore, the transducer signals must be taken off the shaft through slip rings. Both of these factors require that the transducer outputs have a high signal-to-noise ratio. In spite of their poor temperature characteristics, the semi-conductor strain gauges were selected. The temperature characteristics of these gauges are discussed in detail below.

LABORATORY TESTING OF TRANSDUCERS

The transducers were first mounted on a full-scale model of the propeller shaft and tested. This procedure and its results are discussed in Ref. 3, Sec 3.2.6. After the sucessful completion of tests with the model shaft, an entire system of transducers and a slip ring assembly was constructed for installation on the aircraft.

The slip ring assembly and its associated instrumentation are shown in Figs. 9 and 10. This slip ring assembly was designed with great care towards minimizing the noise associated with transferring the signals off the rotating shaft. The entire slip ring asembly including the brushes and their holders was mounted directly on the propeller shaft by bearings. This was done to allow the shaft and the slip ring assembly to vibrate as a single body. This minimized the tendency of the brushes to loose contact with the rings. The brush and ring materials were chosen to minimize the sliding contact noise problem. The brushes were made of silver graphite and the rings of a hard brass alloy. Amplification of the transducer outputs was done in two stages; a first amplification of 1000 was made on the shaft; secondary amplification of 1 to 5 was then made between the slip rings and the recording equipment. The amplification of the signals on the shaft was done to reduce the effect of noise induced in the signals as they pass

through the slip rings. For details of the design and selection procedure of the slip ring assembly, of the electronic amplifiers and signal conditioning instrumentation, and of their installation arrangement on the YO-3A, see Ref. 3, Sec 3.2.6.

The propeller shaft and its pulleys were removed from the aircraft and the transducers and associated instrumentation package were mounted on the shaft in the laboratory. The configuration of the transducers was in the form that it would take on the aircraft. This system was then thoroughly tested in the laboratory, the calibration of these transducers was done both in the labratory, using the arrangement shown in Fig. 11 and 12, and on the aircraft under static conditions. There was no significant difference in the sensitivities found during the laboratory calibration or the aircraft static calibration. In fact the sensitivities, as determined by the calibrations, compared closely with the theoretically expected values listed in Table II. Typical results from these calibrations are illustrated in Figs. 13, 14, 15 and 16.

The effects of internal oil pressure on the transducers were checked during the aircraft static calibration tests. The oil supply line to the propeller shaft was tapped just before it entered the shaft. A pressure pump with an oil reservoir was connected to this line and the effect on the transducers over the range of pressures expected in flight was observed. As expected the internal oil pressure had negligible effect on the output of the transducers. The effect of centrifugal forces generated by shaft rotation was also checked. This also had negligible effect on the transducer outputs.

The effect of temperature change on the transducers was studied in two stages. The preliminary feasibility studies were done in the laboratory. These tests confirmed that the expected range of temperature change had negligible effect on the torque and bending transducers, but had a marked effect on the semi-conductor strain-gauge thrust transducer. These tests were conducted in detail only on the aircraft under static conditions.

The effect of temperature change on the semi-conductor strain-gauges is twofold. Temperature rise causes an increase in the resistance of the strain gauges. This change is given by the following equation.

$$R_t = R_o[1+\alpha_B(T_i-T_o)]$$

where α_B is the bonded coefficent of resistance of the strain gauge and is given by:

$$\alpha_B = \alpha[1+(Cm-Cs)]$$

and α is the temperature coefficent of resistance of the strain gauge

Cm is the thermal expansion coefficent of the metal

Cs is the thermal expansion coefficent of the semi-conductor material

The values of these coefficents for the DGP-1000-500 gauges were

α = .0036 /K, Cm = .000012 /K, Cs = .0000028 /K

Temperature changes also affect the gauge factor of these gauges. An increase in temperature causes a decrease in gauge factor. This effect is given by the following equation

$$G_t = G_o [1+\beta(T_1-T_o)]$$

where β is the temperature coefficent of gauge factor

For the DGP-1000-500 gauges

$$\beta = -.000026 /K$$

The Wheatstone bridge is made up of one such semi-conductor gauge in each arm. The output of this bridge under zero strain changes as the temperature changes because the thermal coefficents of each gauge are not exactly matched (an inherent problem in manufacture). As both the resistance and the gauge factor are functions of temperature, the electrical characteristics of the bridge are also temperature dependent. Any change in temperature causes a change in bridge output voltage. The instrumentation cannot distinguish this output from an output caused by a strain.

These temperature effects on the bridge output can be reduced by adding two compensating resistors to the Wheatstone bridge, the resistance of the compensating resistors being essentially temperature independent.

First, a resistor of appropriate value is placed in parallel with one gauge in the bridge. This reduces the effective resistance, the effective temperature coefficent of resistance, and the effective gauge factor of this gauge. A correctly chosen resistor then keeps the two halves of the bridge in closer balance, and hence reduces the temperature induced output.

The second compensating resistor called a span resistor, is placed in series with the entire bridge. As temperature changes cause a change in the overall bridge resistance, this changes the current drain from the constant voltage power source. The voltage drop across the span resistor changes with the current drain. A correctly chosen span resistor causes the voltage applied across the bridge to compensate for the temperature induced changes in the bridge sensitivity.

The compensating resistor values are a function of temperature and can be determined from the gauge and Wheatstone bridge temperature dependent properties using the above equations. The compensating resistor values therefore can be chosen to null out the no-load temperature induced bridge output at two specific temperatures. One of these is the starting temperature and the other is that elevated temperature for which the compensating resistors were chosen. However, the manufacturer suggests that they be determined experimentally. This was done using the set-up shown in Fig. 17 and 18. The shaft was heated with a heat gun from room temperature up to about 333 K, the expected stable temperature that would be reached in flight. During this heating process, the strain gauge resistances, the bridge voltage output, and the bridge sensitivity changes with temperature were recorded. The temperature was measured at two locations on the shaft by thermistors. The first location was at the position of the thrust bridge and the second location was at the rear of the shaft (these two temperatures gave some idea of the uniformity of applied heat). These thermistor readings were also used to calibrate a thermistor temperature indicating transducer whose voltage output was proportional to temperature. This transducer was for recording the shaft temperature during flight. This sensor was also located at the axial position of the thrust bridge on the shaft. See Figs. 19 and 20 for the actual bridge arrangements on the propeller shaft.

These tests determined the effect of temperature change on the resistance of each gauge, and the bridge output and sensitivity. The results were then used to calculate the thermal coefficents of each gauge and hence to determine the appropriate values of the compensating resistors. These resistor values were then used with the bridge and their values further refined by experimental checking. This whole temperature compensating arrangement for the thrust transducer was thoroughly tested under varying room temperatures. The effect of a summer to winter room temperature change was predictable, i.e. at whatever values the bridge output and resistance started at different room temperatures, they reached the same final values at 333 K.

In the range of temperatures considered, these tests showed that the bridge sensitivity changed negligibly with temperature, but that the bridge resistance changed significantly. No span compensating resistor was needed but a parallel resistor was required to minimize the output voltage changes

The signal-to-noise ratio of the thrust transducer was thus poor. The output had a large temperature dependent component and a somewhat smaller torque dependent component superposed on the basic thrust signal. (The term signal-to-noise ratio as used for the thrust transducer means that the electronic noise as well as the interactions in the basic thrust output, for this application, were all considered to be noise). However these effects were repeatable and could be calibrated.

FLIGHT TEST RESULTS

Several flights were made to measure the thrust and torque acting on the propeller of the YO-3A. During each flight recordings were made of the voltage outputs of the thrust, torque and bending transducers, the temperature transducer voltage output, an electronically generated time reference signal, and the resistances of the two thermistors on the shaft. Since the bending output is periodic at the shaft frequency, the output of the bending transducer along with the time reference signal gave the propeller shaft rotational speed. This speed was confirmed by checking it against the sinusoidal torque and thrust outputs. Altitude, airspeed, outside air temperature, engine manifold pressure, and shaft internal oil pressure as indicated by the aircraft instruments were also recorded. Figure 21 shows the YO-3A ready for a test flight and Fig. 22 shows the recorder mounted in the front cockpit. During repeatability checks, several flights had to be made at the same density altitude.

The atmospheric conditions necessary for reliable in-flight measurements were quite restrictive. Thermal activity could not be tolerated since this causes large changes in the thrust and torque data measured. Due to belt slippage problems at low temperatures the belt drive system proved to be unairworthy for winter ambient conditions. Spring and summer were the only suitable flight test periods available. Finally, since VFR conditions with no precipitation were also essential for flight testing, days suitable for flight testing occurred infrequently.

The data recorded in flight was reduced to International Standard Atmospheric conditions and the thrust and torque as well as the power required and power available were calculated (see Ref. 1 for the reduction procedure). The propeller efficiency was then calculated. The results of the flight tests are presented in Figs. 23, 24, 25 and 26.

These figures show that the torque data is more uniform than the thrust data. This was expected in view of the temperature and torque interactions present in the thrust transducer output and the much higher signal-to-noise ratio of the torque output. The torque component was separated from the thrust signal using the results of the calibrations, but the separation of the temperature dependent component was more difficult.

The temperature compensation, as outlined above, was done on the basis that the main heat source for the shaft was the hot engine oil running through it. The entire temperature compensation was done on the basis of uniform temperature for the whole bridge. However, the in-flight thermistor readings indicated a maximum gradient of 10 K along the shaft. The axial spacing of the thermistors was about ten centimeters. The average temperature gradient hence was 1 K/cm, which was significant for these tests. The four gauges comprising the thrust bridge were not all located at the same axial location. Hence they did not experience the same temperature changes. Each of the two halves of the bridge had strain gauges which were axially separated by about three centimeters. This arrangement was adopted to minimize the effect of the bending interaction on the thrust signal by locating the gauges along the same axial line rather than along the same circumferential location. Hence, the temperature compensation technique described above had to be modified for the effect of the temperature gradient. Observations made

during flight showed that the output of the thrust transducer changed monotonically as the shaft heated up even when the propeller power and the flight conditions were held constant. The shaft reached a stable temperature of about 333 K as allowed for during temperature calibration tests. Under the correct temperature compensation the output would not change monotonically but would reach a maximum and then return towards zero as the shaft reached the stable temperature of 333 K. If the heating of the shaft was partly by conduction of heat from the hot engine compartment, then there would be an axial temperature gradient. This was believed to be the case. As the YO-3A engine overheats very rapidly on the ground , temperature gradient calibrations could not be done on the ground. Further, a temperature gradient induced on the ground would not necessarily be an accurate representation of that encountered in flight.

As a result of the temperature gradient the calibrated correction for the change in thrust output due to temperature could not be used. Instead the effect of temperature on the thrust bridge output was determined analytically. This was based on a knowledge of the shaft temperature gradient measured in flight. Gauge temperatures were based on an assumption of a linear temperature variation along the shaft axis. The gauge temperature coefficents required for this analytic correction were determined experimentally from the measurements made during the temperature compensation calibration tests.

This analytical correction for the bridge output is non-linear and is a function of both the shaft temperature at the gauge location and the temperature gradient between the two axially separated gauges.

This analytical correction was applied to the thrust data and the efficiency calculated on the basis of this thrust data. Figure 24 shows two data points for which calculated efficiency was greater than one. These errors were thought to be wholly or partly due to the approximate nature of the gradient correction made to the thrust data. The normal flight test procedure was to stabilize the aircraft at a particular altitude and at its maximum speed. The aircraft was then decelerated to its stalling speed in small speed decrements. The shaft continously heated during this process and the temperature gradient measured also increased. Hence the data recorded at the earlier stage of the flight

test was at a lower shaft temperature as well as at a smaller temperature gradient. As the analytical correction is based on the assumption of a linear temperature gradient the correction for the earlier data points is less approximate than that for the later ones. The efficiency values calculated for Fig. 24 bear this out as the two points for which the efficiency was calculated to be greater than one were both at low speeds.

CONCLUSIONS

The results of this study show that the instrumentation and procedure developed can be used to measure the torque and with further refinements could be expected to satisfactorily measure thrust on the YO-3A.

The primary problem encountered in the thrust measurement was the temperature gradient effect which caused non-uniform temperatures in the thrust bridge. This problem can be eliminated by arranging the thrust bridge so that each of its strain gauges is at the same axial location on the shaft. This however will result in higher bending interactions in the thrust signal. Unlike the temperature gradient correction this interaction can be corrected for by a calibration procedure similar to that employed for the torque interaction. With this arrangement the bridge can then be temperature compensated using the procedure outlined in this study.

The other problem encountered in this study was that the thrust strain levels were extremely low. The weak link mechanical strain intensifier approach studied here could probably be refined to solve this problem. Some structural modifications to the propeller shaft would be required for attaching this transducer. Since this transducer amplifies the low thrust strains mechanically, foil strain gauges could be used. These gauges have no adverse temperature characteristics. The weak link should be located near the shaft axis to prevent amplification of torque and bending strains. If the shaft so allows this transducer could be placed inside the shaft. Alternatively such a transducer could also be placed in the thrust load path between the propeller hub and the shaft.

REFERENCES

1. Condon, G. W., Rundgren, I. W., and Davis, W. B., 'Army Preliminary Evaluation I,YO-3A Airplane, Final Report', US ARMY Aviation Systems Test Activity, August 1970.

2. Vogley, A. W., 'Climb and High-Speed Tests of a Curtis No. 714-1C2-12 Four-Blad Prop on the Republic P-47C Airplane', NACA ACR No. L4L07, 1944.

3. Ormsbee, A. I., Sivier, K. R., Siddiqi, S. A., Woan, C. J., Plencner, R. M., 'Development of Criteria for Design of a Low Noise Level General Aviation Propeller', PROGRESS REPORT, Aeronautical and Astronautical Engineering Department, University of Illinois at Urbana-Champaign.

LIST OF SYMBOLS

A	cross-section area in m^2
E_o	output voltage of a strain gauge bridge
I	section moment of inertia in m^4
J	section polar moment in inertia in m^4
K_g	gauge factor of a strain gauge, i.e., unit resistance change per unit strain
M	bending moment in m-N
Q	torque in m-N
R	resistance in ohms
T	thrust load in N
V	bridge excitation voltage
ε	strain in microstrains
ε_B	bending induced strain
ε_Q	torque induced strain
ε_T	thrust induced strain
σ	stress in Pascals, Pa
μ	Poisson's Ratio

Maximum Load	Section Characteristics	Strength of Section	Strain Equation	Strain Per Unit Load & Maximum Strain	Stress Per Unit Load & Maximum Stress
Thrust T_{Max} = 2200N	$A = 1.22 \times 10^{-3} m^2$	$AE = 254.5 \times 10^{6} N$	$\varepsilon_T = \frac{T}{AE}$	$\frac{\varepsilon_T}{T} = .00395$ micro-strains/N $\varepsilon_{T_{Max}} = 9$ micro-strains	$\frac{\sigma_T}{T} = 820\ m^{-2}$ $\sigma_{T_{Max}} = 1.83$ MPa
Torque Q_{Max} = 1600 m-N	$J = .86 \times 10^{-6} m^4$	$JG = 6.36 \times 10^{4} m^2\text{-}N$	$\varepsilon_Q = \frac{QR}{2JG}$	$\frac{\varepsilon_Q}{Q} = .236$ micro-strains/m-N $\varepsilon_{Q_{Max}} = 375$ micro-strains	$\frac{\sigma_Q}{Q} = 34.96 \times 10^{3} m^{-3}$ $\sigma_{Q_{Max}} = 55.3$ MPa
Bending M_{Max} = 180 m-N (at bearing end of the shaft)	$I = .43 \times 10^{-6} m^4$	$IE = 8.93 \times 10^{4} m^2 N$	$\varepsilon_B = \frac{MR}{IE}$	$\frac{\varepsilon_M}{M} = .336$ micro-strains/m-N $\varepsilon_{M_{Max}} = 60$ micro-strains	$\frac{\sigma_B}{M} = 69.6 \times 10^{3} m^{-3}$ $\sigma_{B_{Max}} = 11.84$ MPa

TABLE I

PROPELLER SHAFT LOADS

Sensor Arrangement	dε/dT	Full Scale $\varepsilon_{T_{Max}}$	dε/dQ	Full Scale $\varepsilon_{Q_{Max}}$	% Interaction $\frac{\varepsilon_{Q_{Max}}}{\varepsilon_{T_{Max}}} \times 100$
Mech. Strain Intensifier (weak link transducer)	.056 μV/V/N	125 μV/V	.17 μV/V/m-N	266 μV/V	212%
Foil Bridge on shaft	.0054 V/V/N	12.0 μV/V	.0071 μV/V/m-N	11.34 μV/V	94%
Semi-Cond. Bridge on Shaft	.35 μV/V/N	780 μV/V	.176 μV/V/m-N	280μV/V	36 %
Torque Bridge on Shaft	---	40 micro-strains 20 μV/V	1.054 micro-strains/ m-N	1680 micro-strains 840 μV/V	< 2.5%

TABLE II

SENSOR EVALUATION TEST RESULTS

Figure 1. The YO-3A Aircraft with Cowl Removed

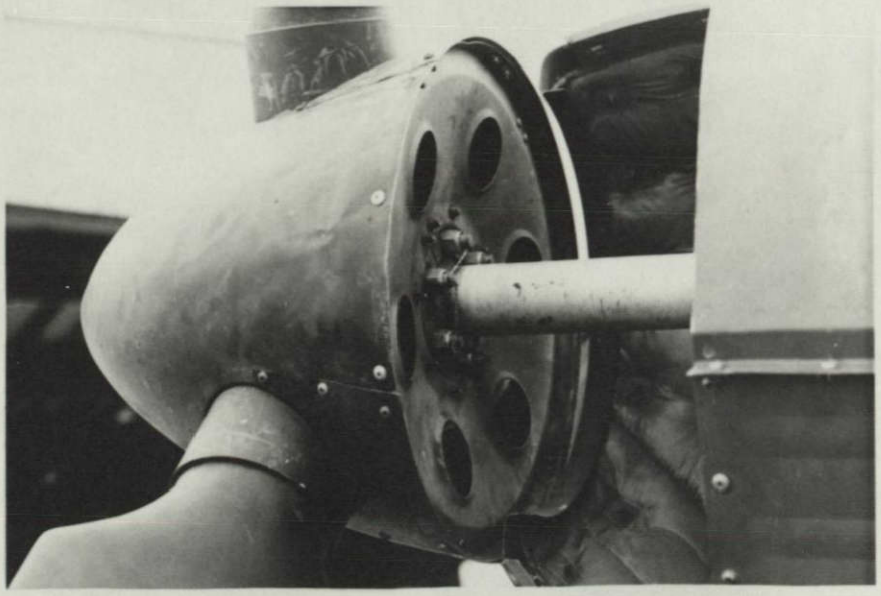

Figure 2. The YO-3A's Propeller Shaft and Hub

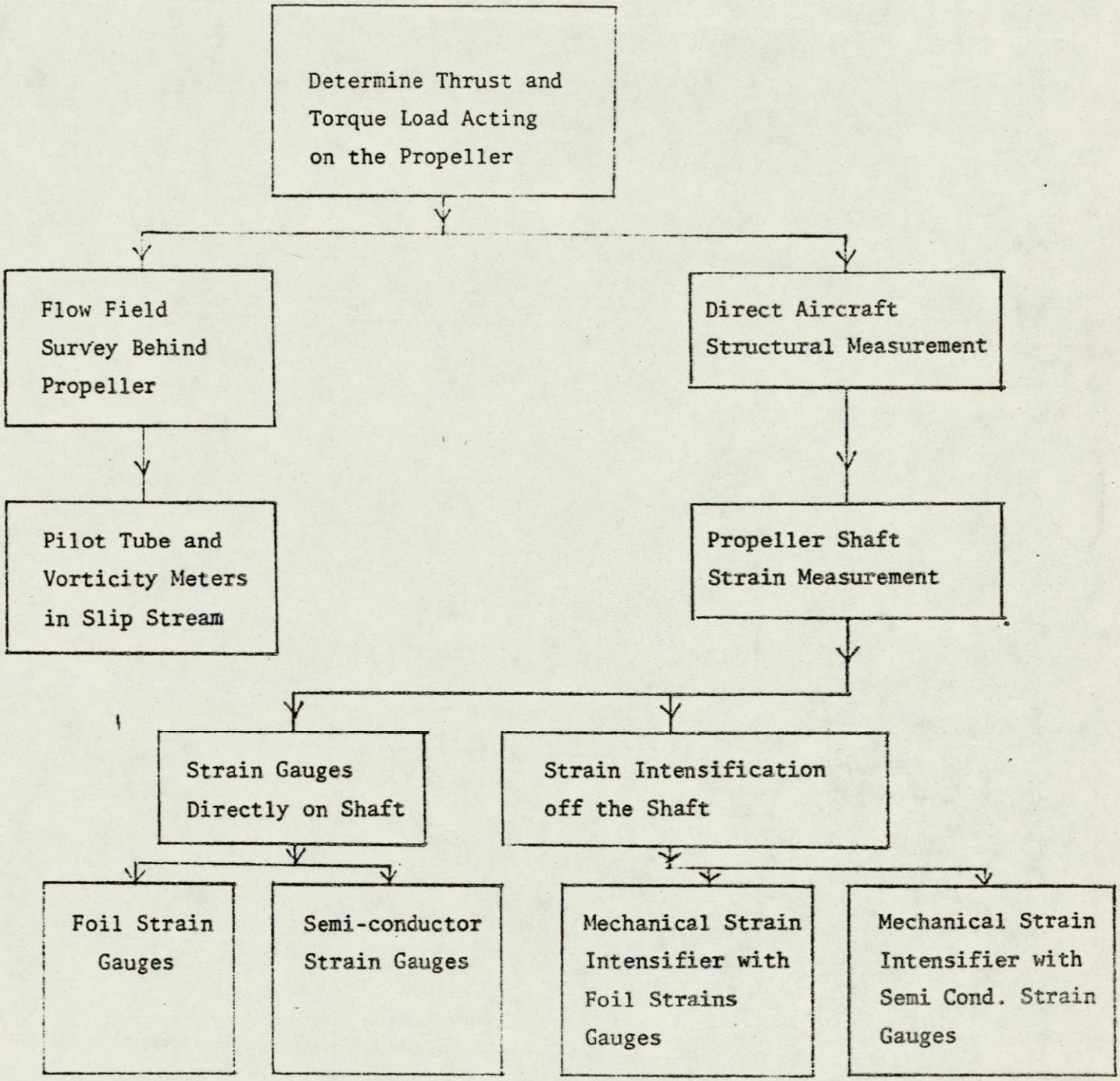

Figure 3. Approaches to the In-Flight Measurement of Propeller Performance

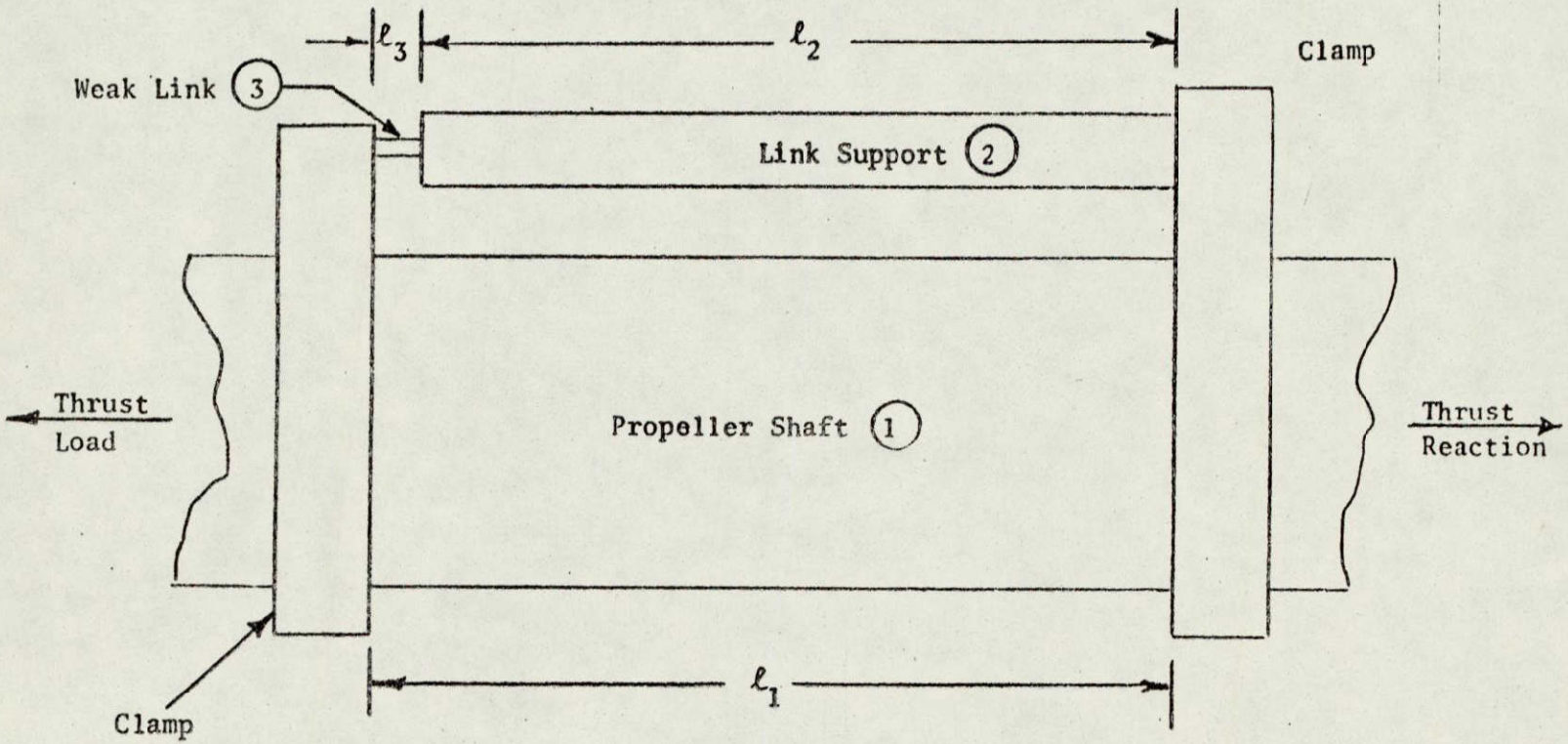

Figure 4. Schematic of Mechanical Strain Intensifier

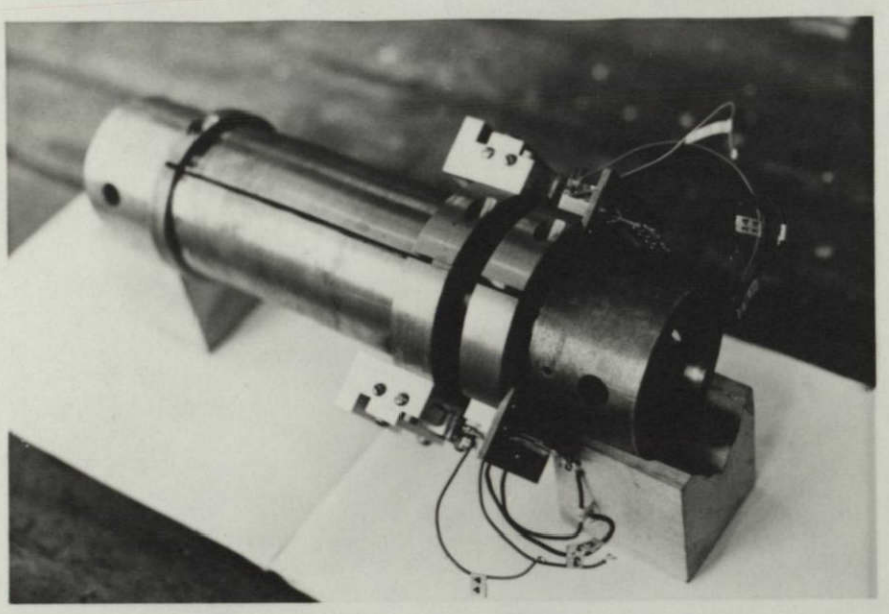

Figure 5. The Weak Link Transducer

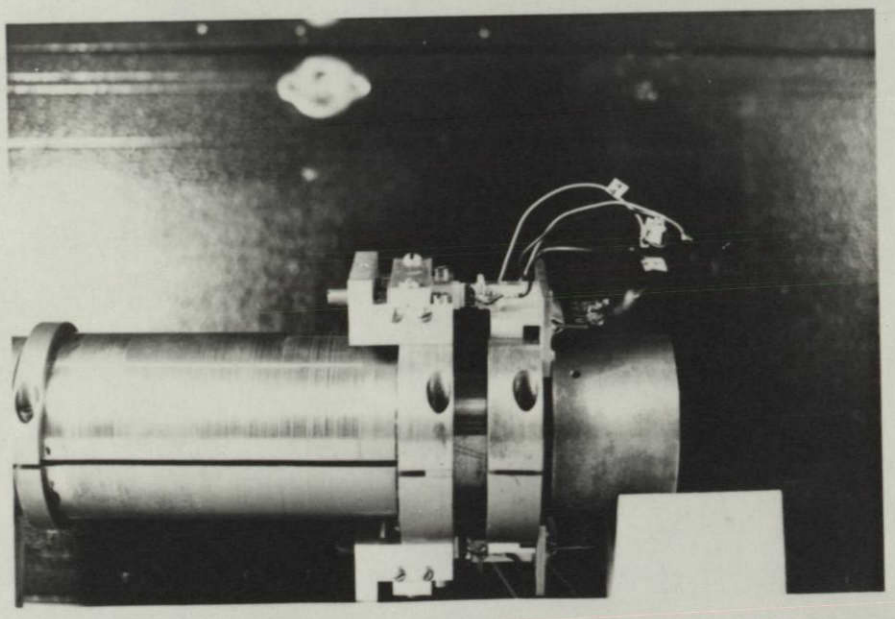

Figure 6. The Weak Link Transducer

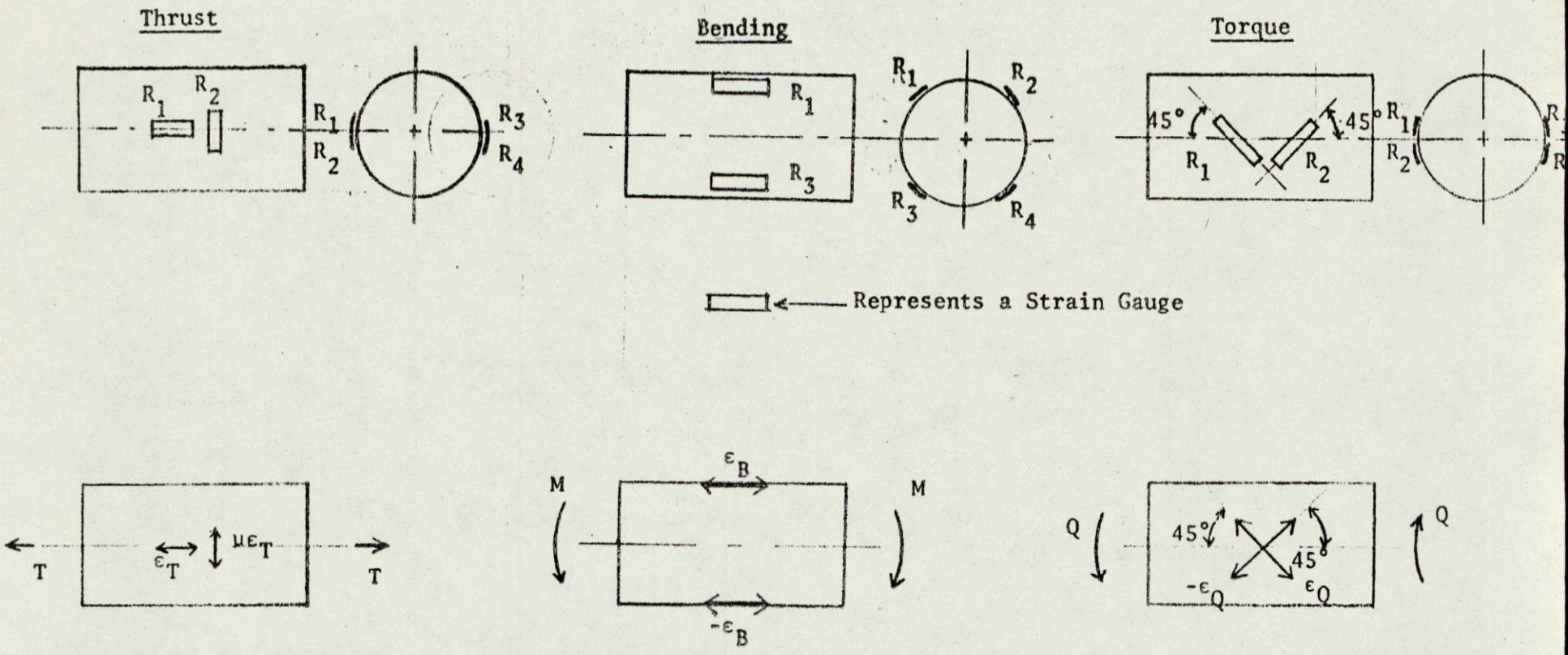

Figure 7. Propeller Shaft Strain Gauge Arrangements and Strain Directions

Thrust

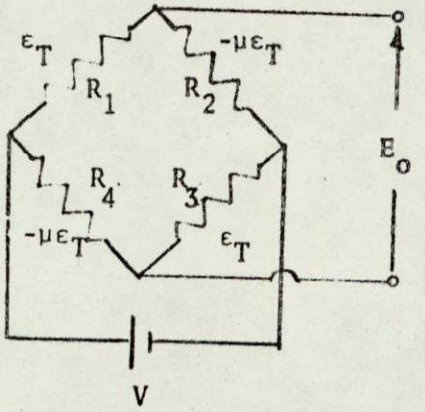

μ = Poisson's ratio of the shaft material

μ = 0.3 for steel

$E_o = \frac{Kg}{4}[2(1+\mu)\varepsilon_T]V$

Bending

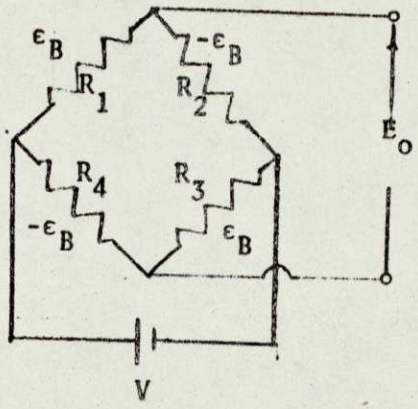

$E_o = \frac{Kg}{4}[4\varepsilon_B]V$

Torque

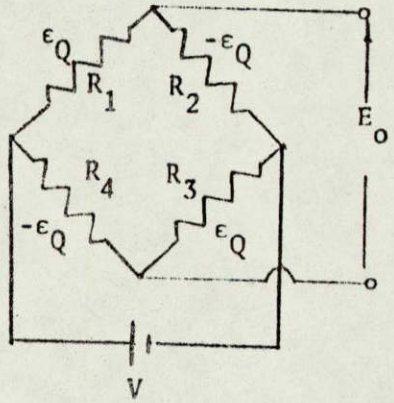

$E_o = \frac{Kg}{4}[4\varepsilon_Q]V$

Figure 8. Thrust, Bending and Torque Strain Bridge Circuits

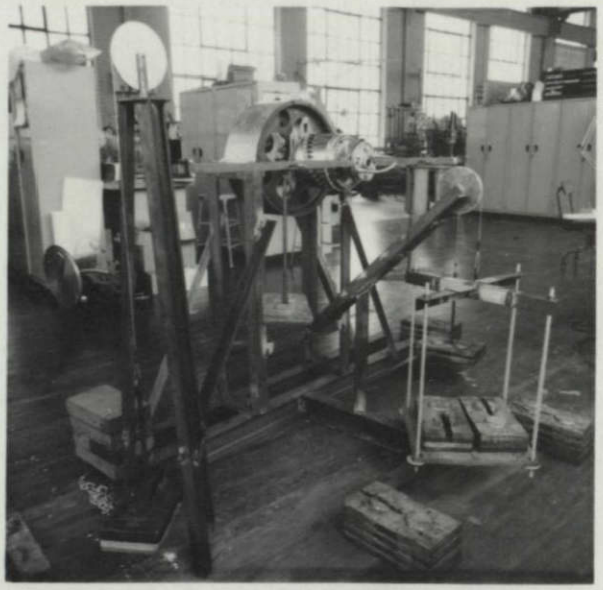

Figure 11. Laboratory Combined Loading Arrangement

Figure 12. Instrumentation and Recorder with the Combined Loading Arrangement

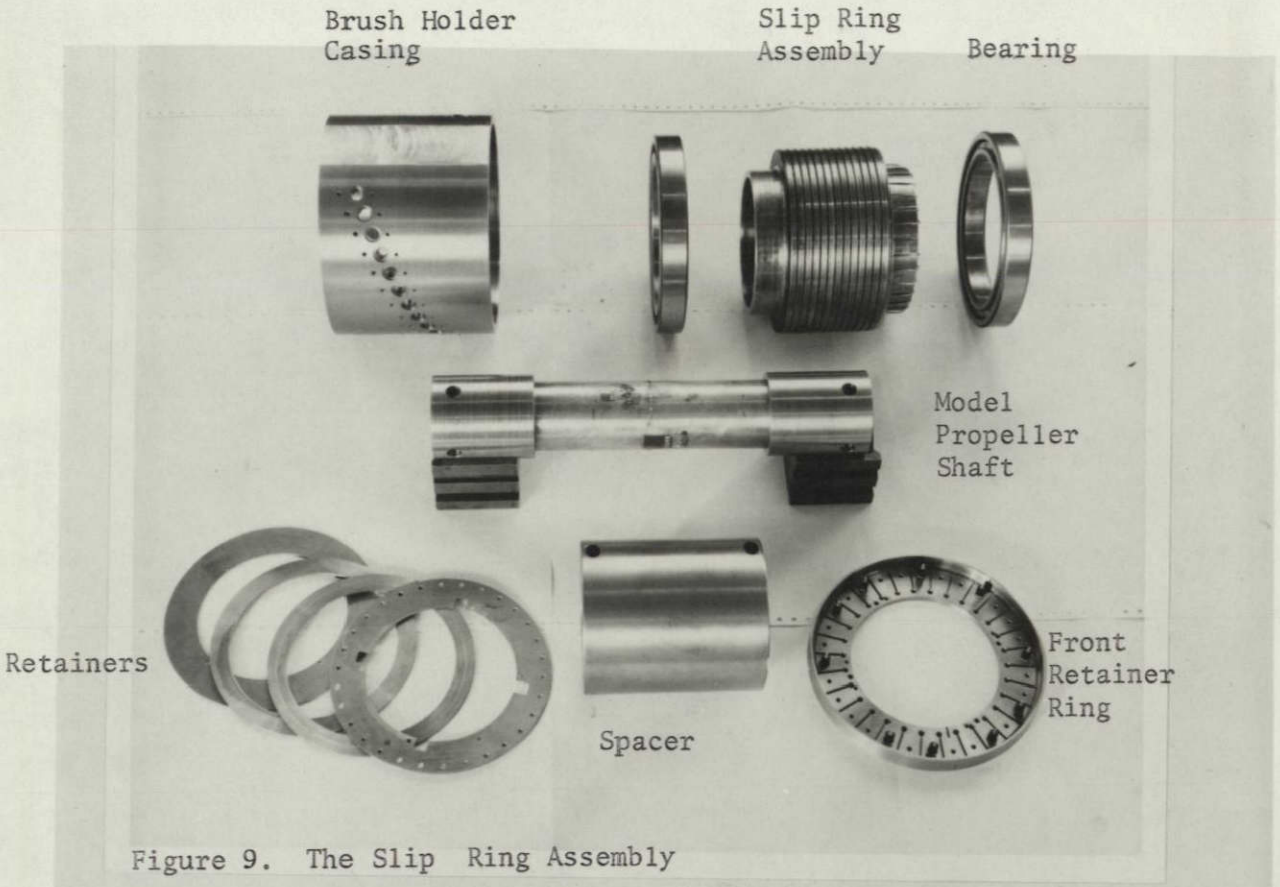

Figure 9. The Slip Ring Assembly

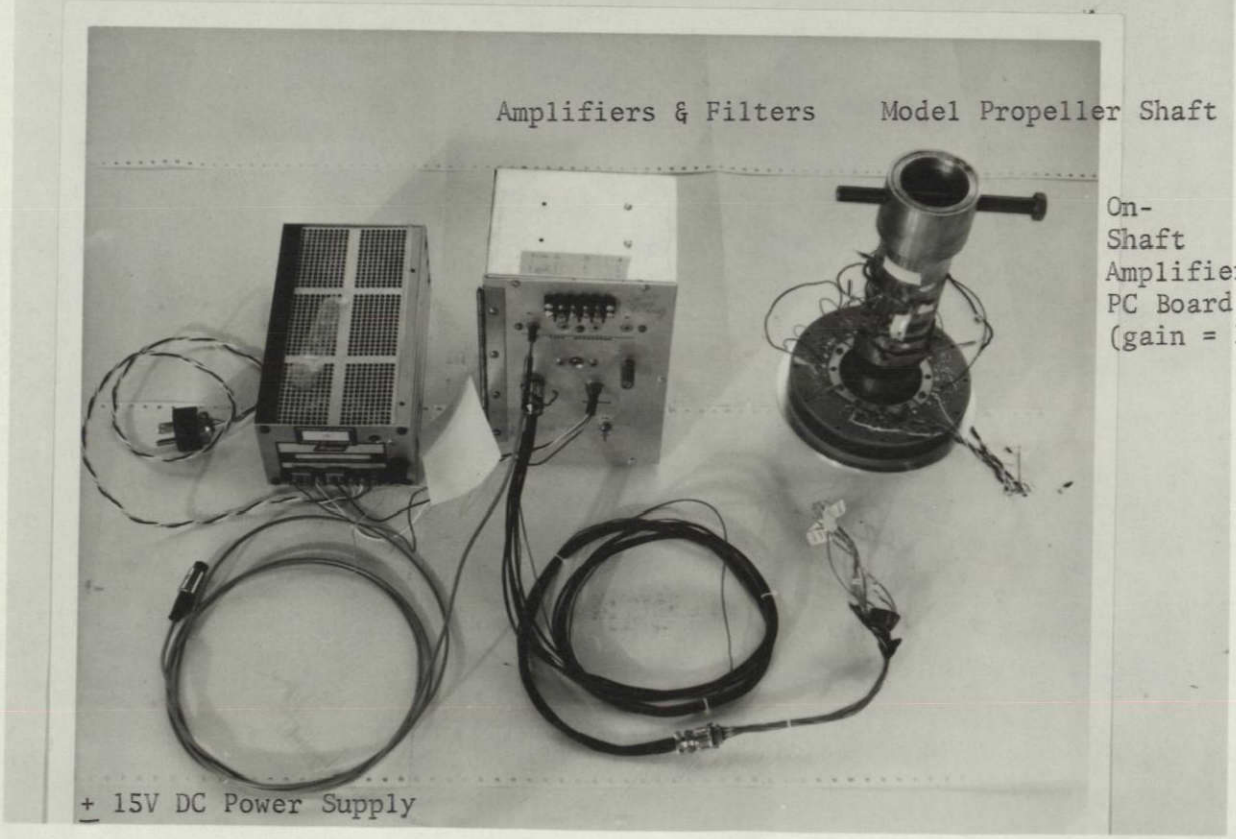

Figure 10. The Instrumentation System

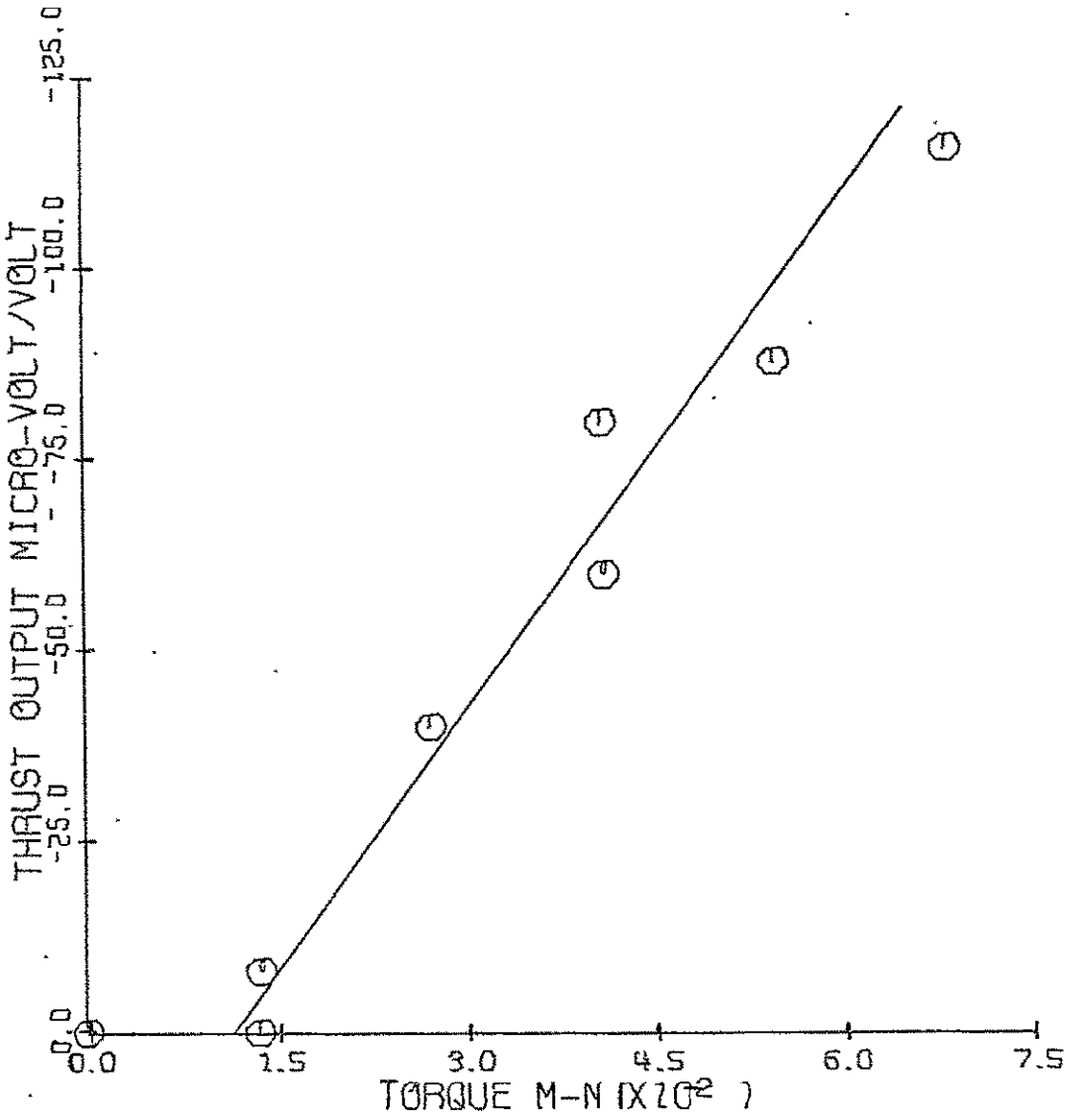

FIG. 14 PLOT OF THRUST OUTPUT VERSUS TORQUE LOAD

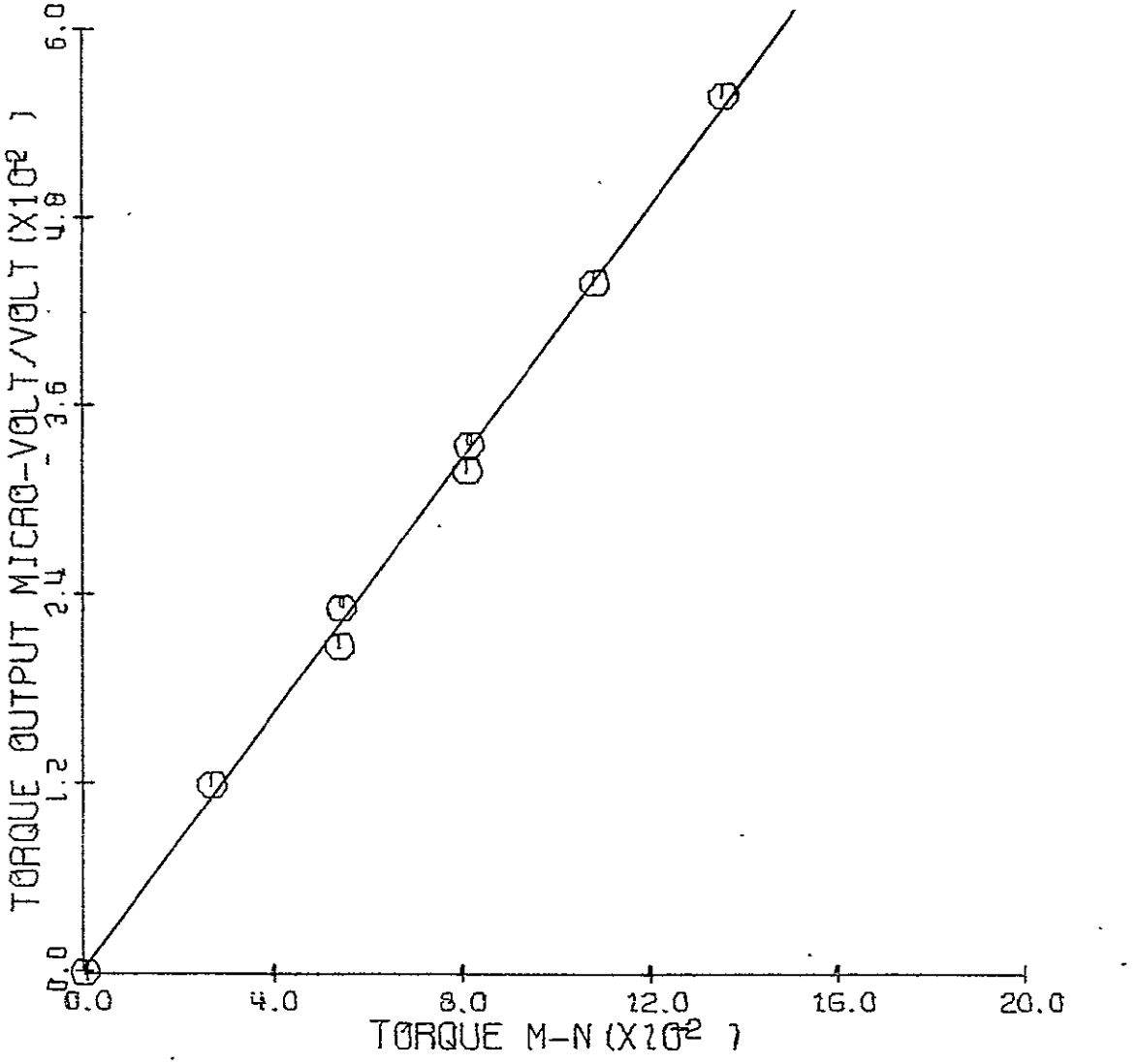

FIG. 15 PLOT OF TORQUE OUTPUT VERSUS TORQUE LOAD

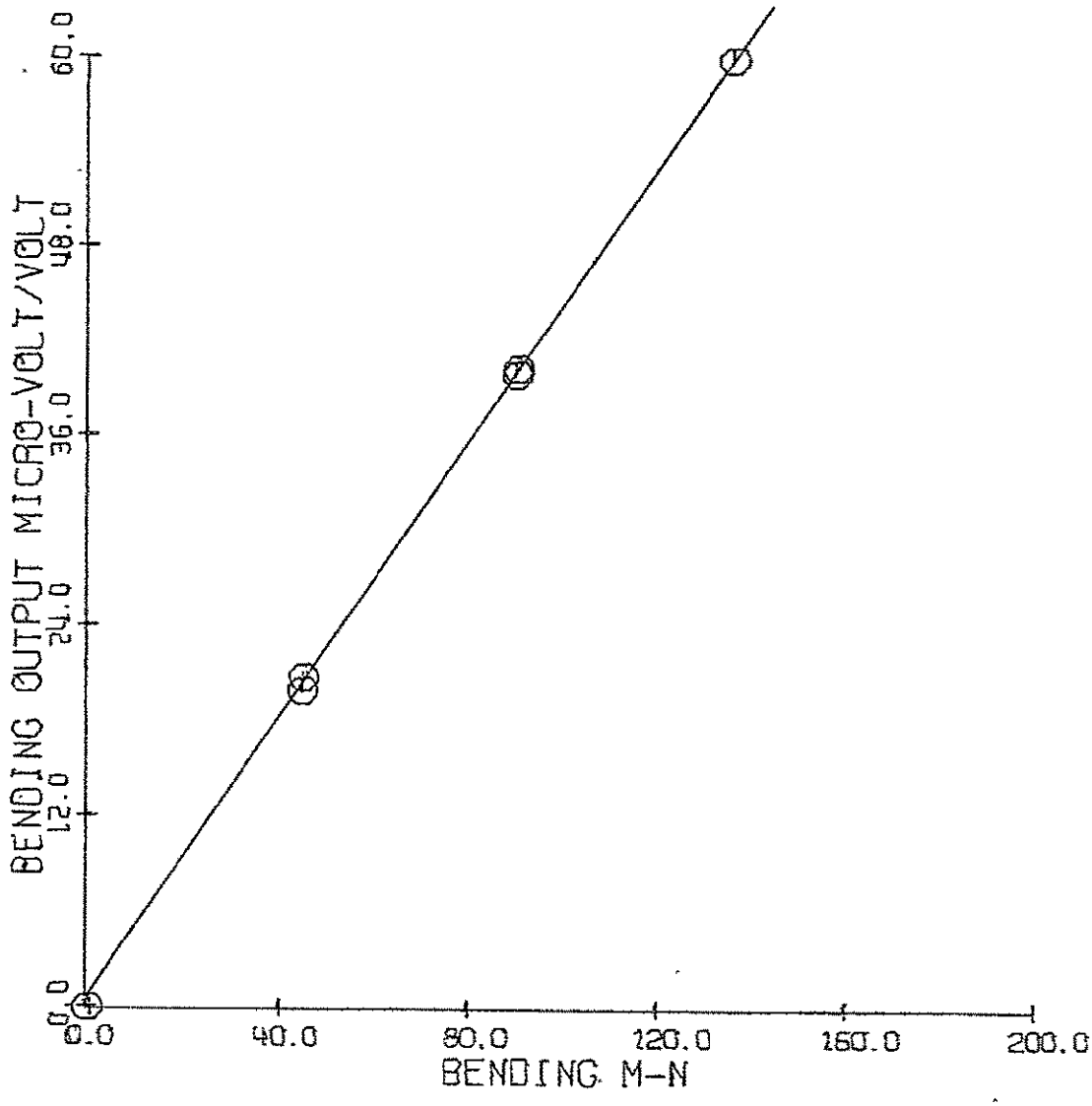

FIG. 16 PLOT OF BENDING OUTPUT VERSUS BENDING LOAD

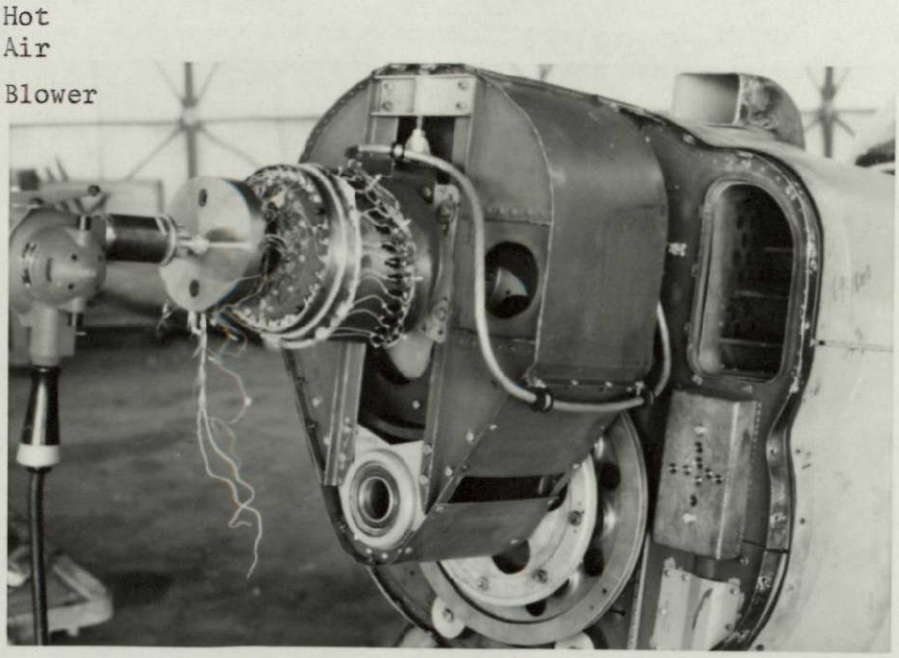

Figure 17. Propeller Shaft Heating Arrangement

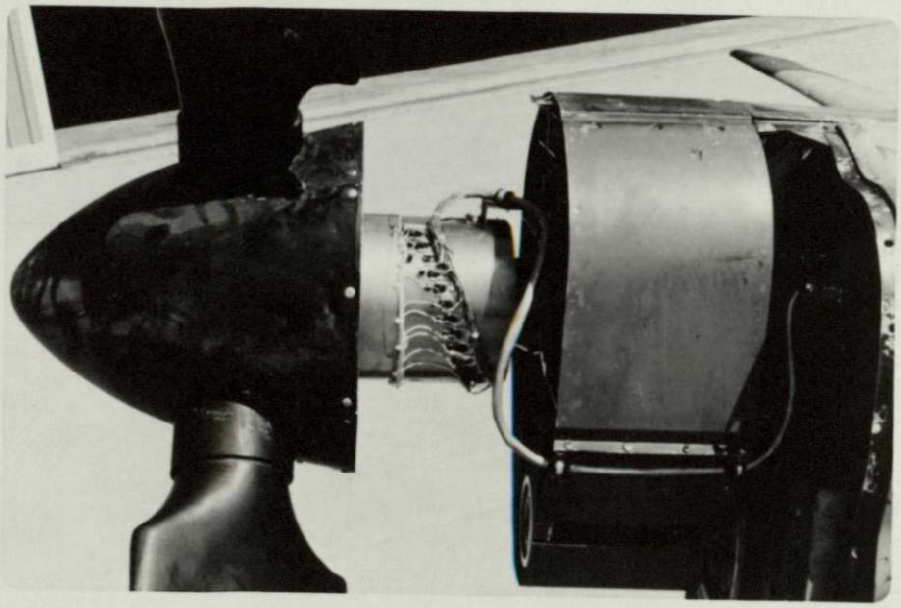

Figure 18. The Slip Ring Assembly Mounted on the YO-3A

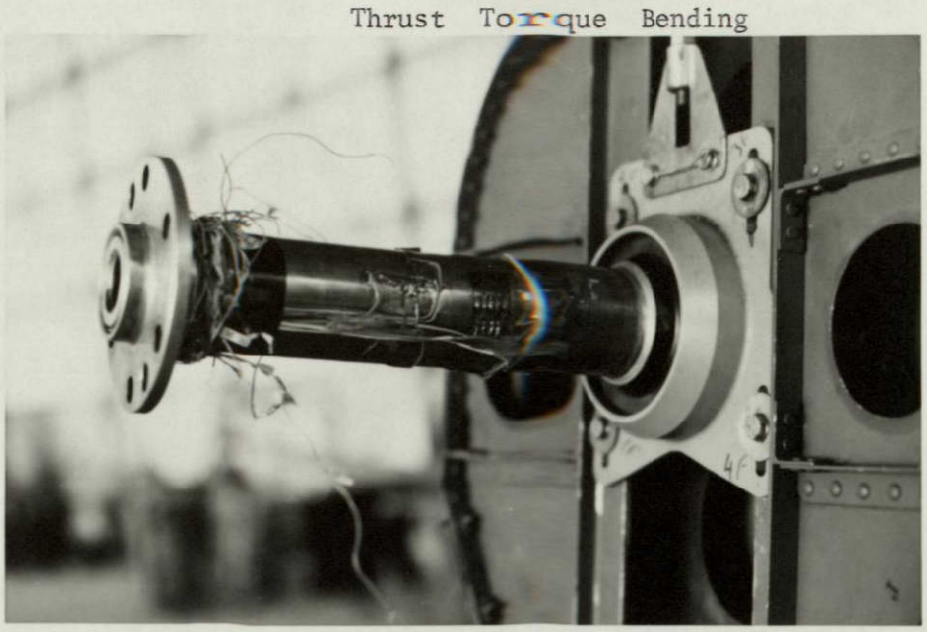

Figure 19. Strain Gauged Propeller Shaft

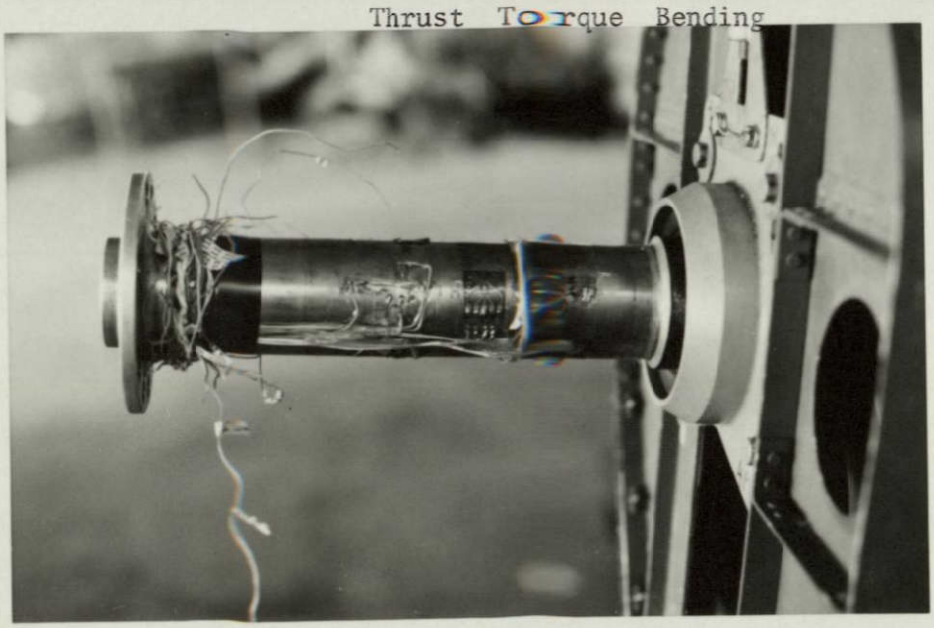

Figure 20. Strain Gauged Propeller Shaft

Figure 21. The YO-3A Ready for Flight Testing

Figure 22. Instrumentation for Flight Tests in the Front Cockpit

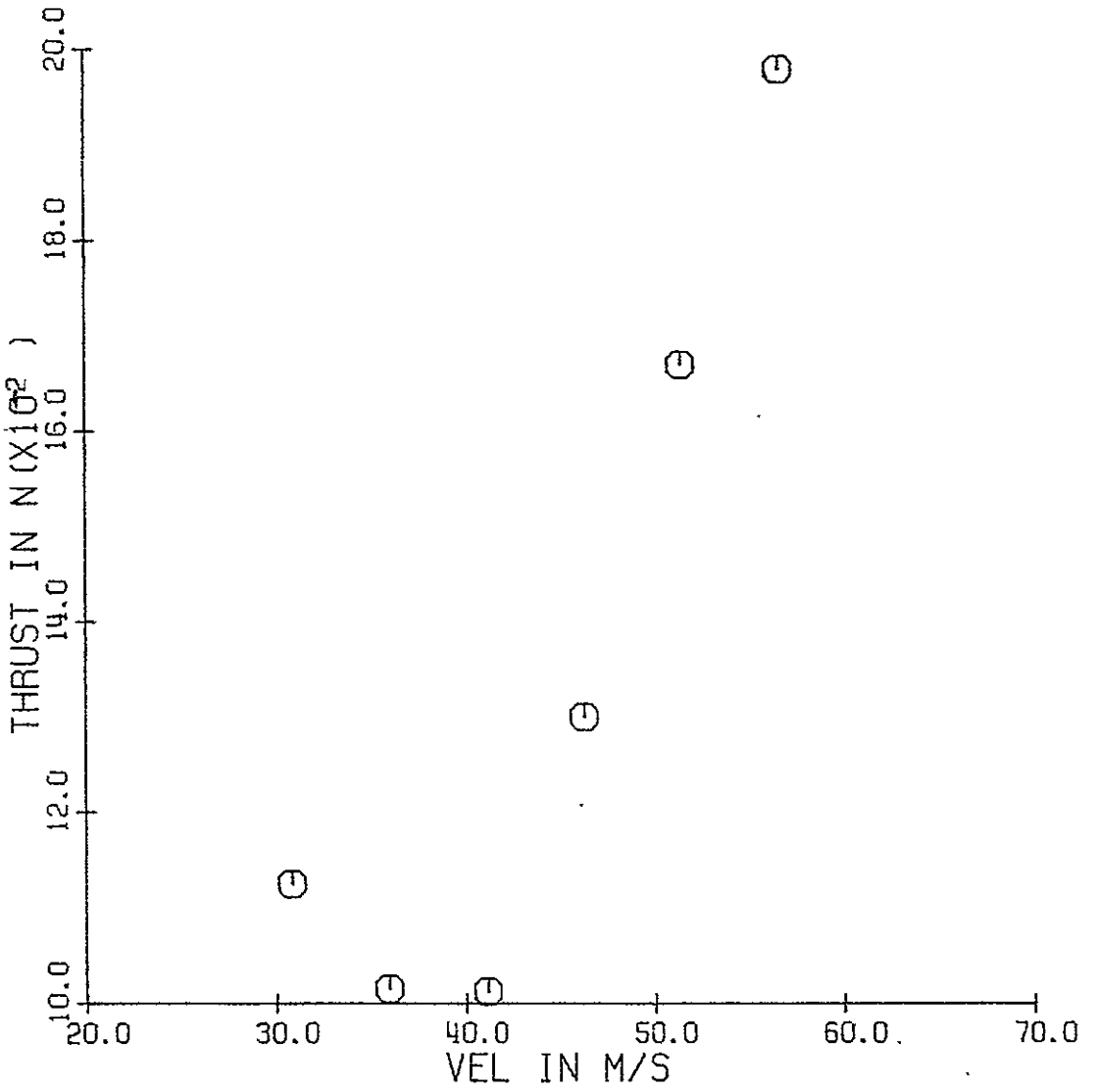

FIG. 24 PLOT OF THRUST VERSUS VELOCITY

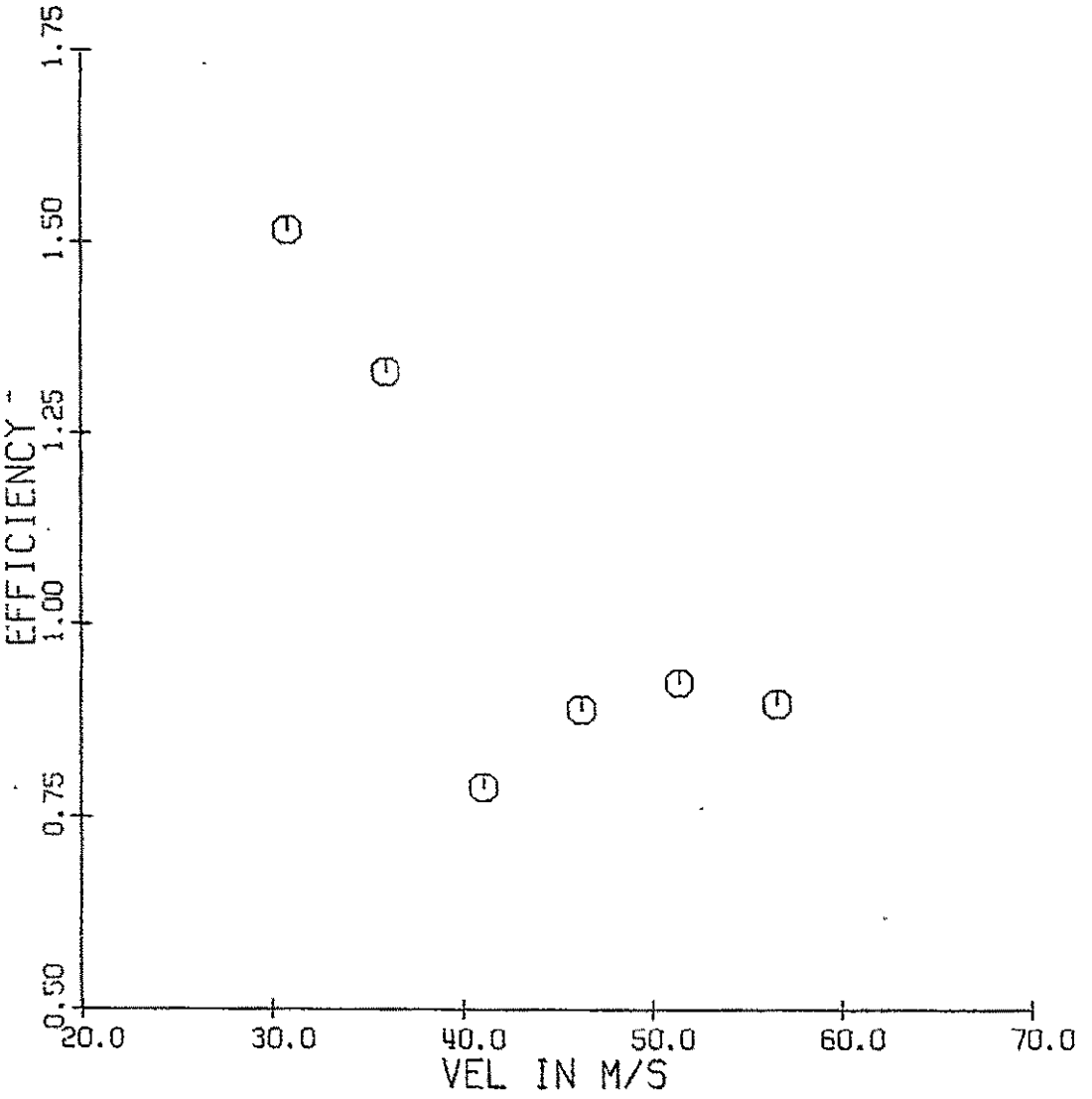

FIG. 25 PLOT OF EFFICIENCY VERSUS VELOCITY

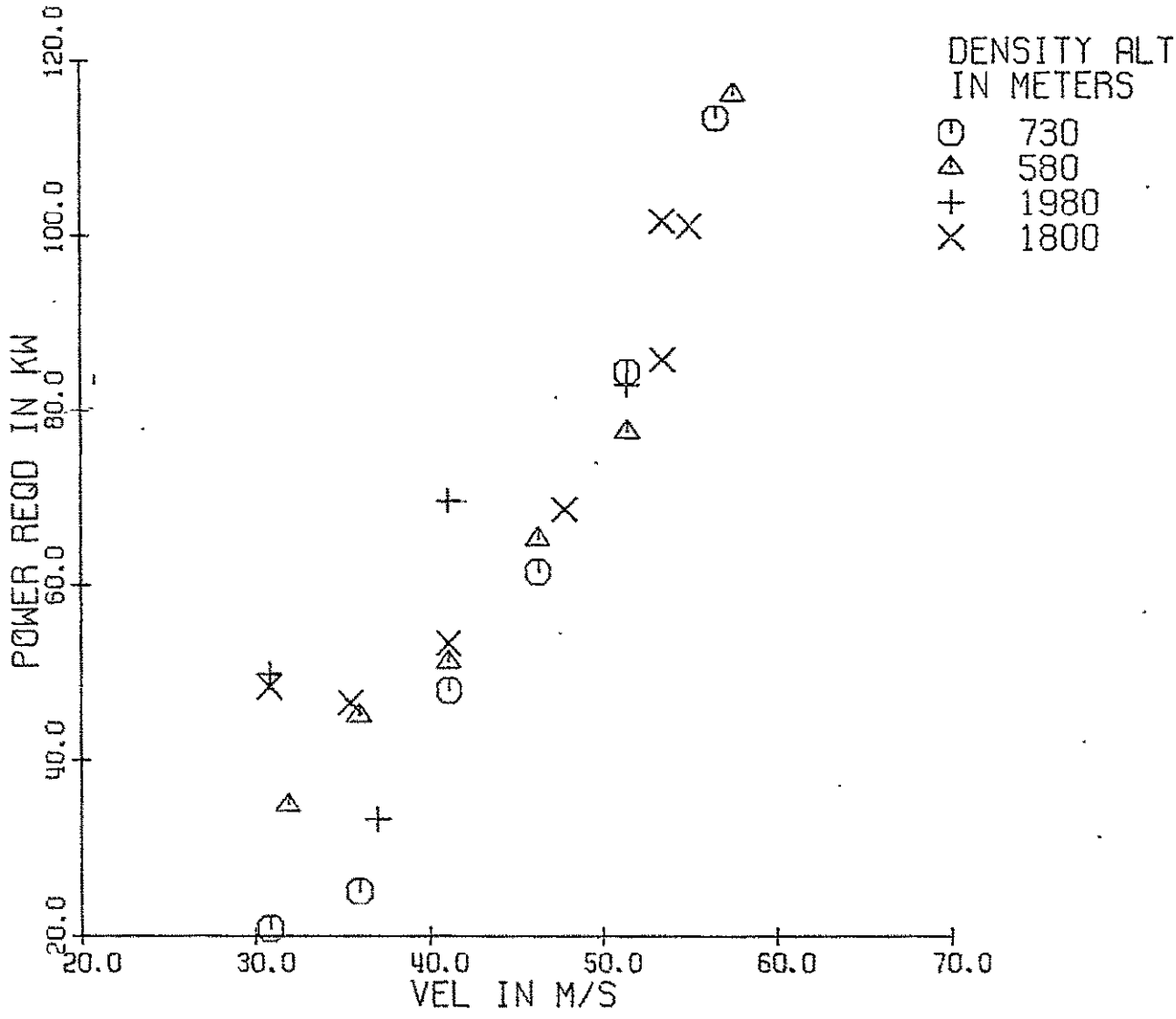

FIG. 26 PLOT OF POWER AVAILABLE VERSUS VELOCITY